Spectral prediction model for variable dot-size printers

Fabrice Rousselle, Thomas Bugnon, Roger D. Hersch; Ecole Polytechnique Fédérale de Lausanne (EPFL); Lausanne, Switzerland

Abstract

By printing a variable number of droplets onto the same pixel location, ink jet printers produce pixels at variable dot-sizes yielding several darkness levels. Varying the number of printed droplets affects the ink volume deposited onto the substrate. In the present contribution, we explore the possibility of producing accurate spectral reflectance predictions at all pixel dot-sizes. For this purpose, we use a Clapper-Yule model, extended according to Beer's law, which accounts for ink thickness variations. This model expresses each colorant transmittance as a function of its constituent ink transmittances and their respective relative thicknesses. These relative thicknesses are initially computed when calibrating the model, at a given pixel dot-size, and can then be dynamically scaled according to the printed pixel dot-size. We first study the effect of varying pixel dot-sizes on the halftone's physical (mechanical) dot-gain. We then express the ink volume variations as a function of pixel dot-sizes. Lastly, we show how, using the thickness extended Clapper-Yule model, we can effectively predict reflectances for different configurations of ink pixel dot-sizes.

Introduction

Among the many printing technologies, ink jet is widely used. In recent ink jet printers, multiple darkness levels per pixel are obtained by varying the number of ink droplets, *i.e.* varying the ink volume. The larger the deposited volume, the darker the printed pixel dot. The Canon i990 printer, used to produce all results presented in this paper, enables printing with 8 different dot-sizes.

No classical reflectance or color prediction model supports variations in ink volumes. An accurate spectral reflectance prediction model accounting for variable dot-size would be very useful for designing new color separation strategies exploiting the high potential offered by variable dot-size printers. Note that Yang [7] modeled solid ink and colorant layers printed at variable dot sizes by using the Kubelka-Munk model and by assimilating ink volume variations to ink thickness variations.

In this work we propose to model the effect of variable dot-sizes. To do so, we use a modified Clapper-Yule model taking into account ink thicknesses. By considering a printed halftone dot as a perfect cylinder of a fixed diameter, we can effectively model volume variations by thickness variations. After calibration of the model, it is then possible to account for the ink volume variations induced by the pixel dot-size variations. We start by describing the classical Clapper-Yule model and its extensions. We then analyse the physical halftone dot gain at different ink dot-sizes. We also express effective ink volume variations as a function of printed ink dot-sizes. We then measure the accuracy of spectral predictions obtained using the thickness enhanced spectral reflectance prediction model when applying the same dot-size variation to every ink. Then, in order to validate our model, we deduce ink volume variations and evaluate reflectance predictions for the general case, where the pixel dot-size differs for each ink. Finally, we draw the conclusions.

The Clapper-Yule based spectral prediction model

The Clapper-Yule model [2] is the only classical halftone spectral reflectance prediction model incorporating the notion of colorant transmittance. It models the multiple internal reflections occurring at the interface between the print and the air. Since we modify the printed pixel dot-sizes, and therefore the colorant transmittances, this model is of particular interest. For 3 inks, *i.e.* 8 Neugebauer primaries (colorants), the Clapper-Yule formula is:

$$R(\lambda) = K \cdot r_s + \frac{(1-r_s) \cdot r_g \cdot (1-r_i) \cdot \left(\sum_{j=1}^{8} a_j \cdot t_j\right)^2}{1 - r_g \cdot r_i \cdot \sum_{j=1}^{8} a_j \cdot t_j^2} \tag{1}$$

where K is the fraction of specularly reflected light reaching the spectrophotometer, r_s is the specularly reflected light, $r_g(\lambda)$ is the paper substrate reflectance, r_i is the internal reflection at the print-air interface, a_j is the jth colorant's surface coverage and $t_j(\lambda)$ is the jth colorant's transmittance [4].

Hersch et al. [4] proposed two extensions to the Clapper-Yule model. Their first extension concerns the notion of ink spreading (physical dot-gain). Because of ink spreading, the effective surface coverage of an ink halftone is generally larger than its nominal surface coverage. In previous spectral prediction models [1], ink spreading was computed for inks printed directly on paper and the resulting ink spreading was assumed to be valid for inks printed in superposition of one or two inks. In practice, ink spreading depends on whether the ink is printed on paper, in superposition of a specific ink or in superposition with two specific inks. Consider the three standard inks, cyan, magenta and yellow, and their respective nominal surface coverages, noted c, m and y. Using the Demichel equations, we obtain the 8 colorants surface coverages, cyan (a_c), magenta (a_m), yellow (a_y), red (a_r), green (a_g), blue (a_b), black (a_k) and white (a_w):

$$
\begin{array}{ll}
a_c = c \cdot (1-m) \cdot (1-y); & a_m = (1-c) \cdot m \cdot (1-y) \\
a_y = (1-c) \cdot (1-m) \cdot y; & a_r = (1-c) \cdot m \cdot y \\
a_g = c \cdot (1-m) \cdot y; & a_b = c \cdot m \cdot (1-y) \\
a_k = c \cdot m \cdot y; & a_w = (1-c) \cdot (1-m) \cdot (1-y)
\end{array}
\tag{2}
$$

There are 12 superposition conditions: cyan halftone alone (c), cyan halftone with solid magenta (c/m), cyan halftone with solid yellow (c/y), cyan halftone with solid magenta and solid yellow (c/my), magenta halftone alone (m), magenta halftone with solid cyan (m/c), magenta halftone with solid yellow (m/y), magenta halftone with solid cyan and solid yellow (m/cy), yellow halftone alone (y), yellow halftone with solid cyan (y/c), yellow halftone with solid magenta (y/m) and yellow halftone with solid cyan and solid magenta (y/cm). The ink halftone effective surface coverages are noted c', m' and y'. The functions mapping nominal to effective surface coverages for superpositions with paper, one ink and two inks are respectively

noted f_i, $f_{i/j}$ and $f_{i/jk}$. The effective surface coverages are defined by the following equations:

$$c' = f_c(c)(1-m')(1-y') + f_{c/m}(c)m'(1-y')$$
$$+ f_{c/y}(c)(1-m')y' + f_{c/my}(c)m'y' \qquad (3)$$

$$m' = f_m(m)(1-c')(1-y') + f_{m/c}(m)c'(1-y')$$
$$+ f_{m/y}(m)(1-c')y' + f_{m/cy}(m)c'y' \qquad (4)$$

$$y' = f_y(y)(1-c')(1-m') + f_{y/c}(y)c'(1-m')$$
$$+ f_{y/m}(y)(1-c')m' + f_{y/cm}(y)c'm' \qquad (5)$$

This system can be solved iteratively. We first set c', m' and y' to the nominal values c, m and y. The system stabilizes after a few iterations, typically 4 to 5. We then compute the effective colorant surface coverages (a'_w, a'_c, a'_m, a'_y, a'_r, a'_g, a'_b, a'_k), using the Demichel equations (Equations 2).

The second extension addresses the assumption of the Clapper-Yule model, that the probability of light exiting from a given colorant is equal to that colorant coverage. In practice, for lower screen frequencies, the probability of light exiting from the same colorant it entered is higher than the colorant surface coverage. To account for this fact, the model extension assumes that a fraction b of the emerging light exits from the same colorant it entered. This fraction is predicted using a Saunderson corrected Neugebauer model. The Neugebauer model [5] assumes that light always exits from the same colorant it entered. It simply sums the reflectance of all colorants, weighted according to their area coverage. By expressing a colorant reflectance according to the Saunderson correction [6] accounting for multiple internal reflections, we obtain the Saunderson corrected Neugebauer model. In this extended Clapper-Yule model, the fraction b predicted using the Saunderson corrected Neugebauer model corresponds to light propagated along short distances. The fraction $(1-b)$ predicted by the Clapper-Yule model corresponds to light propagated along middle to long distances. The resulting prediction model, hereafter called the *original extended* Clapper-Yule model is:

$$R(\lambda) = K \cdot r_s + (1-r_s) \cdot r_g \cdot (1-r_i) \left[b \sum_{j=1}^{8} \frac{a_j \cdot t_j^2}{1 - r_i \cdot r_g \cdot t_j^2} \right.$$
$$\left. + (1-b) \frac{\left(\sum_{j=1}^{8} a_j \cdot t_j \right)^2}{1 - r_g \cdot r_i \sum_{j=1}^{8} a_j \cdot t_j^2} \right] \qquad (6)$$

We now introduce the *thickness extended* Clapper-Yule model [3]. It accounts for the thickness of each ink by relying on Beer's law:

$$t(\lambda) = \exp^{-\xi \cdot d \cdot k(\lambda)} \qquad (7)$$

where ξ is the concentration of the ink colorant, d its thickness, and k its spectral absorption coefficient. According to Equation (7), scaling the thickness of an ink of transmittance $t(\lambda)$ by a factor s yields a transmittance $t(\lambda)^s$.

Since the Clapper-Yule model is based on colorant transmittances, let us first express a colorant transmittance using its constituent inks transmittances as well as their corresponding ink thickness scaling factors. Consider a colorant AB, formed by two inks A

and B. Its transmittance is equal to the product of each ink transmittance, scaled by their respective relative thicknesses, noted d_{Ab} and d_{aB}. For three or more inks, we proceed in an analog manner:

$$t_{AB} = t_A^{d_{Ab}} \cdot t_B^{d_{aB}}$$
$$t_{ABC} = t_A^{d_{Abc}} \cdot t_B^{d_{aBc}} \cdot t_C^{d_{abC}} \qquad (8)$$

For colorant *AB*, thicknesses d_{Ab} and d_{aB} are called *initial thicknesses* and they are computed when calibrating the model. We first deduce both the ink transmittances and the colorant transmittances from their reflectances, measured on solid patches, using the classical Clapper-Yule formula. The initial thicknesses are then fitted by minimizing the sum of square differences between the deduced colorant transmittance and the one predicted from deduced ink transmittances, according to Equation (8).

In the thickness extended model, a colorant transmittance is replaced by its constituent ink transmittances. The resulting approximated colorant transmittance however is slightly different from the colorant transmittance deduced from the measured reflectance. This difference may be due to the fact that the Clapper-Yule model does not consider penetration of ink into the paper bulk. Since ink penetrates differently when printed alone or in superposition with other inks, the approximated colorant transmittance differs from the one deduced from the reflectance measurement. For example, with the print used to calibrate the model in the next section, we obtain CIELAB ΔE_{94} color difference values of 2.02, 1.88, 1.21 and 0.57 for colorants blue, red, green and black respectively, between deduced and approximated transmittances.

Pixel dot-size variations induce ink volume variations, which we express as *thickness variations*. According to Beer's law, if the thicknesses of inks A and B in colorant AB are respectively scaled according to factors s_a and s_b, we have:

$$t_{AB} = \left(t_A^{d_{Ab}} \right)^{s_a} \cdot \left(t_B^{d_{aB}} \right)^{s_b} = t_A^{d_{Ab} \times s_a} \cdot t_B^{d_{aB} \times s_b}$$
$$t_{ABC} = \left(t_A^{d_{Abc}} \right)^{s_a} \cdot \left(t_B^{d_{aBc}} \right)^{s_b} \cdot \left(t_C^{d_{abC}} \right)^{s_c} = t_A^{d_{Abc} \times s_a} \cdot t_B^{d_{aBc} \times s_b} \cdot t_C^{d_{abC} \times s_c}$$
$$(9)$$

At this point, let us note that, according to Beer's law (Equation 7), varying an ink thickness by a factor s has the same effect as varying its concentration by the same factor s. In practice, the inks forming a colorant do not necessarily form distinct layers but are often blended together. Nevertheless, since concentration variations have the same effect as thickness variations, Equation (9) holds.

The thickness extended model allows us to dynamically account for variations of an ink's thickness. It also allows detection of a variation of an ink's thickness, by comparing predicted and measured reflection spectra [3].

Ink spreading in function of dot-size

In this section, we analyse halftone ink spreading in function of printed pixel dot-size. For this analysis, we use, at each pixel dot-size, the original extended Clapper-Yule model, shown in Equation (6), with colorant transmittances deduced from reflectance measurements of colorants printed at the corresponding pixel dot-size and with the b factor set to 0.1.

All test patches are printed with a Canon i990 printer using standard cyan, magenta and yellow inks at a resolution of 600 dpi

and a screen frequency of 100 lpi. This printer is capable of printing at 8 different pixel dot-sizes. We chose to calibrate the model at dot-size 4, which yields the calibration print noted C4M4Y4. This notation is used throughout the paper and gives the first letter of the ink name (C, M and Y for cyan, magenta and yellow), followed by the dot-size. The test consists of varying each ink dot-size individually, while keeping the other two inks at the calibration dot-size. For the magenta case, we have the following prints: C4M1Y4, C4M2Y4, C4M3Y4, C4M4Y4, C4M5Y4, C4M6Y4, C4M7Y4 and C4M8Y4. The prints are made of 125 patches, showing the 125 combinations of ink superpositions for variations of nominal halftone surface coverages of 0, 0.25, 0.5, 0.75 and 1.

The fitted halftone dot-gains obtained at different printed pixel dot-sizes are shown in Figure 1 (next page). We note that, for superposition with paper, magenta and yellow, the dot-gain curves are similar at all dot-sizes. Only the superpositions with cyan or with two other inks yield significantly different dot-gain curves.

Expressing relative volume variations as a function of pixel dot-sizes

Ink volume variations, obtained by varying the printed pixel dot-sizes, affect both the halftone dot thickness and its surface coverage. In the present approach, we compute the volume variations by maintaining the halftone dot surface coverages constant and by fitting only the thickness variations. The volume variation can either be a nominal value, given by the printed dot-size, or an effective value, fitted from measured reflection spectra. The nominal volume variation is obtained by dividing the printed dot-size by the chosen calibration dot-size. Since we use a calibration printed dot-size of 4, the nominal volume variations for dot-sizes $[1, 2, 3, 4, 5, 6, 7, 8]$ are $[0.25, 0.50, 0.75, 1.00, 1.25, 1.50, 1.75, 2.00]$.

The fitted, or effective, volume variations are obtained by minimizing the difference between 125 predicted and measured spectra. We use the sum of square differences as a minimization metric. In order to characterize the volume variations, we use test prints at each available pixel dot-size: C1M1Y1, C2M2Y2, C3M3Y3, C4M4Y4, C5M5Y5, C6M6Y6, C7M7Y7 and C8M8Y8. In total we have 8 prints, each with 125 patches, showing all possible ink superpositions with coverages of 0, 25, 50, 75 and 100%. The resulting volume variations, are expressed in Figure 2 by the percentual gain in respect to the nominal volume variation. The fitted ink volume variations used to produce this figure are given in the Appendix, Table A, "fully fitted variations".

In practice, we can interpolate between the ink volume variations at dot-size 1, dot-size 4 and dot-size 8 to create a similar function mapping nominal pixel dot-sizes to ink volume variations. The print at the calibration dot-size, C4M4Y4, is used to calibrate the thickness extended Clapper-Yule model. The two other prints, at dot-size 1 and dot-size 8, are used to deduce volume variations. To fit the volume variations, we only use a subset of 12 patches (from the 125 available). These 12 patches are the superpositions of an ink at 50% coverage with paper and with solid colorants. For example, with cyan, we have 50% cyan on paper, 50% cyan on solid magenta, 50% cyan on solid yellow and 50% cyan on solid red. Using the fitted volume variations at dot-sizes 1 and 8, and using a volume variation of 1 (*i.e.* no variation) at the calibration dot-size, we interpolate the volume variations at all other dot-sizes. These interpolated volume variations are called *partially fitted* variations, in contrast to the *fully fitted* variations obtained when considering all 125 patches at
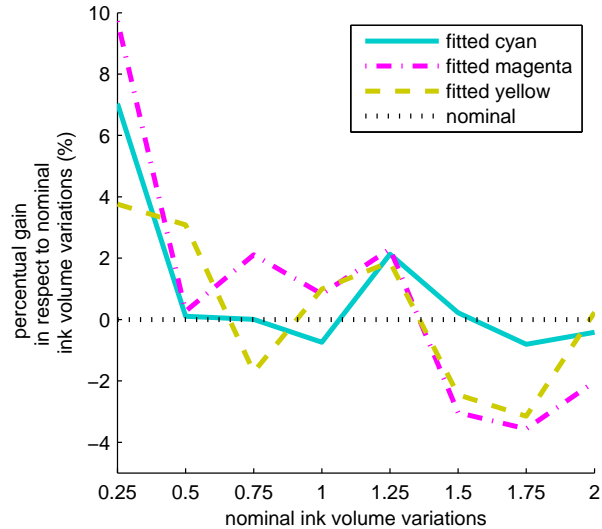

Figure 2. Relative gain of fitted volume variations, in respect to nominal volume variations, for dot-sizes [1, 2, 3, 4, 5, 6, 7, 8], using print C4M4Y4 to calibrate the model. The values used to produce this figure are given in Table A (Appendix).

every dot-size. The next section presents results obtained using both partially and fully fitted volume variations.

Spectral reflectance predictions at varying pixel dot-sizes

We apply the thickness extended model for the forward prediction, *i.e.* for predicting the reflection spectrum of a halftone patch knowing the nominal ink coverages and the pixel dot-size, *i.e.* its nominal ink volume variation. To measure the accuracy of our predictions, we compute the ΔE_{94} distance between predicted and measured spectra. As previously, we use dot-size 4 to calibrate the model. Test prints comprise all possible dot-sizes: C1M1Y1, C2M2Y2, C3M3Y3, C4M4Y4, C5M5Y5, C6M6Y6, C7M7Y7, C8M8Y8. Using the thickness extended Clapper-Yule model, calibrated for a dot-size of 4, predictions are made using nominal, fully fitted and partially fitted volume variations. Using the same model, but recalibrated for each pixel dot-size, reference predictions are obtained. The resulting ΔE_{94} distances (averaged over all patches for each print) are given in Figure 3.

The results show that, when increasing the dot-size, the reference prediction accuracy decreases and the standard deviation increases (Figure 3, red curve). This is most likely due to an accentuated dot-gain at larger dot-sizes inadequately handled by the original extended Clapper-Yule model. The behavior of the thickness extended model is similar for fitted volume variations (blue and green curves). Also, we note that predictions obtained using nominal and fitted volume variations are comparable. This is expected since, as we can see in Figure 2, the fitted volume variations are very close to the nominal ones.

In order to appreciate the benefit of the thickness extended model, let us show the predictions achieved without accounting for pixel dot-size variations. For this purpose, we use the original extended model calibrated with the print C4M4Y4 and compare its spectral reflectance predictions with the measured patch re-
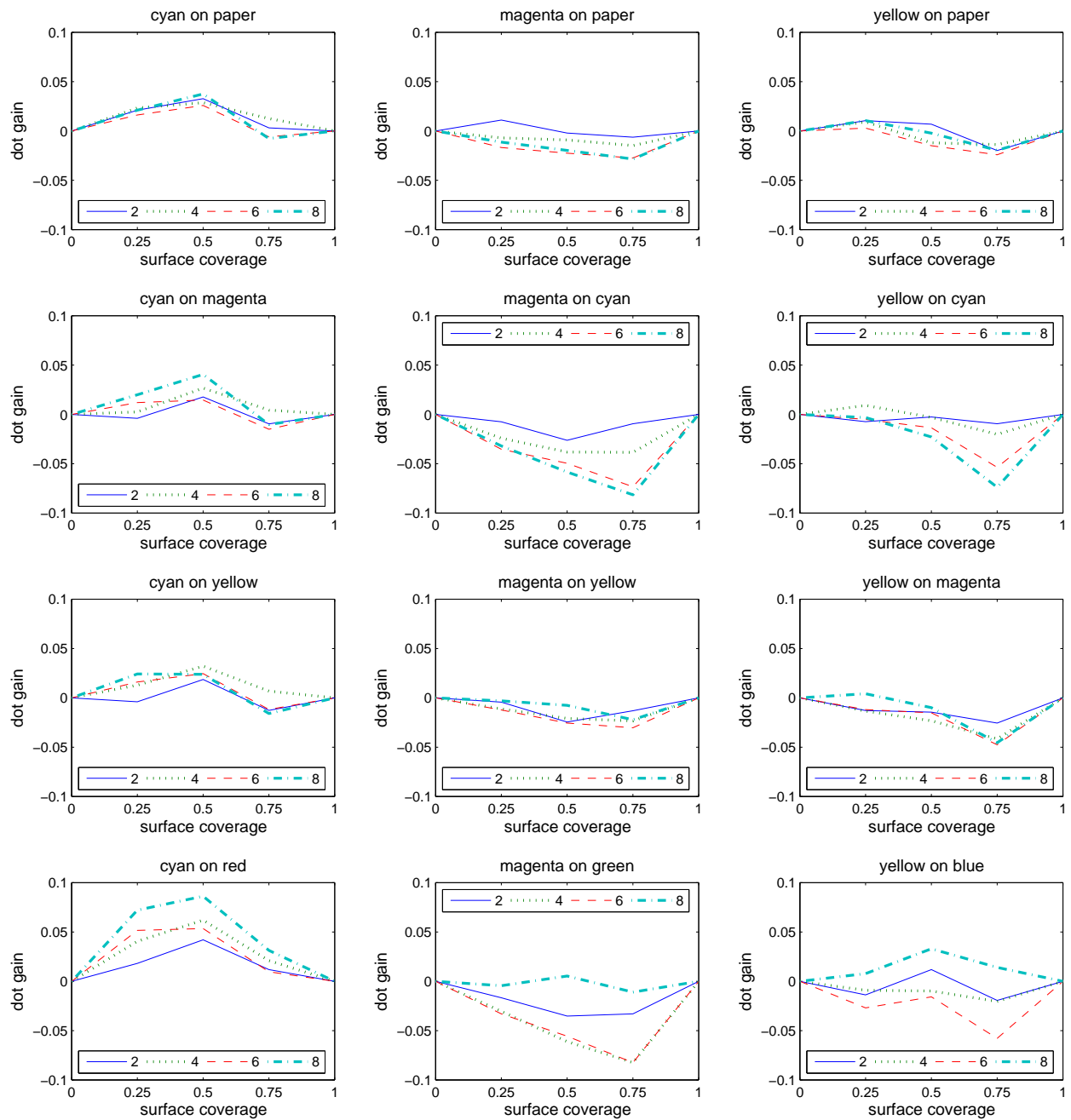
Figure 1. *Physical halftone dot gains fitted from reflectances, for different cyan, magenta and yellow printed pixel dot-sizes. The dot gain is defined as the halftone effective surface coverage minus its nominal surface coverage. Values are computed using the extended Clapper-Yule model with $b = 0.1$. For clarity, only the curves at dot-sizes 2, 4, 6 and 8 are given.*
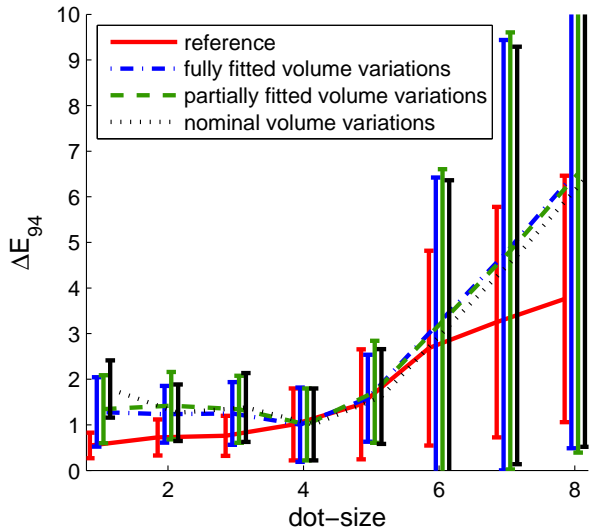
Figure 3. *Mean prediction accuracy, according to the ΔE_{94} metric, using the thickness extended model calibrated with print C4M4Y4. The reference predictions, shown in red, are obtained by recalibrating the model specifically for each pixel dot-size. The values used to produce this figure are given in Table C (Appendix).*

Figure 4. *Mean prediction accuracy, according to the ΔE_{94} metric, using the original extended model, i.e. without taking ink volume variations into account, calibrated for print C4M4Y4. The reference predictions, shown in red, were obtained by recalibrating the model specifically at each pixel dot-size. The values used to produce this figure are given in Table B (Appendix).*

flectances. We also produced reference predictions using the same model, but calibrated specifically for each pixel dot-size. The resulting prediction errors, according to the ΔE_{94} metric, are given in Figure 4. The prediction error is significantly higher when decreasing the dot-size, than when increasing it. Interestingly, variations to smaller dot-sizes are very well handled by the thickness extended model, with no significant decrease of prediction accuracy. This implies that the dot-size reduction has effectively been accounted for by the proposed ink volume variations model.

Validation

In the previous two sections, we considered the same printed pixel dot-size for all inks. This does not represent the general case, where each ink pixel dot-size can be set to different values. Consequently, in this section, we study different printed pixel dot-sizes for the different inks, *e.g.* a C1M5Y3 print of our 125 test patches. We use a two step approach. In the first step we verify how accurately we can fit the effective ink volume variations from the 12 calibration patches. In the second step, we predict the reflectance spectra of the test patches.

In Figure 2, we showed the relation between dot-size variations and volume variations, by fitting the volume variation minimizing the distance between measured and predicted spectra. While still using the thickness extended model calibrated for print C4M4Y4, we now fit the volume variations for print C1M5Y3. Performing the minimization between predicted and measured reflectance spectra, we obtain the fitted volume variations $[0.28, 1.22, 0.74]$ for nominal values $[0.25, 1.25, 0.75]$. These variations are close to the ones given in Figure 2, $[0.27, 1.28, 0.74]$, which were computed from prints for which we applied the same volume variation to each ink.

For our second test, we predict the reflectance spectra of all test patches of the C1M5Y3 print. The ΔE_{94} distance between predicted and measured spectra is then computed. The prediction is carried
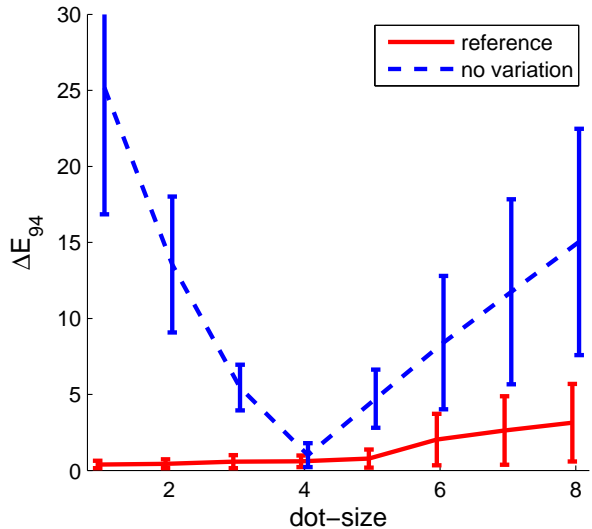
out using both nominal and fitted volume variations according to the Appendix, Table A. Reference predictions are obtained by specifically calibrating the model with print C1M5Y3. The table below lists the average distance between measured and predicted spectra for the 125 test patches. While the average ΔE_{94} distance is similar for nominal and fitted volume variations, the 95% quantile error is lower when using fitted variations. We note that the accuracy of the predictions obtained using fitted volume variations is reasonably close to the accuracy of reference predictions.

Prediction accuracy using nominal, fully fitted and partially fitted volume variations.

	ΔE_{94}			
	mean	max	95% quantile	RMS
reference	1.19	3.21	2.60	0.0096
nominal	1.35	3.85	3.01	0.0133
fully fitted	1.38	3.49	2.74	0.0110
partially fitted	1.32	3.73	2.78	0.0105

Conclusion

Among the classical spectral reflectance prediction models, the Clapper-Yule model is particularly interesting. It is the only model applicable to halftone prints which accounts explicitly for the colorant transmittances. Combined with a Saunderson corrected Neugebauer model and using the ink spreading equations proposed by Hersch et al., it can achieve very accurate predictions. It can also be easily extended to account for ink thickness variations, thereby widening its scope of applicability.

We used the thickness extended Clapper-Yule model for predicting reflectance spectra at the various dot-sizes offered by the Canon i990 inkjet printer. When calibrating the model at dot-size 4 for each ink, which is in the middle of the range of 1 to 8 offered

by this printer, we are able to keep the same level of prediction accuracy when decreasing the dot-size. On the other hand, the prediction accuracy decreases rapidly when increasing the dot-size. This may be due to an inherent weakness of the thickness extended Clapper-Yule model at very large pixel dot-sizes.

We see three primary axes for future research. The first two concern the classical Clapper-Yule model itself. We could first investigate the degradation of prediction accuracy at larger dot-sizes. Then, we could consider the interaction between the ink and the substrate, in order to improve the accuracy of the colorant transmittances and their approximation using their constituent ink transmittances [8]. Finally, considering our tests which showed that halftone dot-gain can be significantly affected for certain superposition conditions when varying the pixel dot-size, it would be interesting to explore varying both the thickness and the surface coverage of halftone dots, when fitting volume variations.

Appendix: Volume variations and prediction accuracy

A. Nominal, fully fitted and partially fitted volume variations, with respect to print C4M4Y4.

dot-size	2	4	6	8	
nominal	0.50	1.00	1.50	2.00	
cyan	0.50	0.99	1.50	1.99	fully
magenta	0.50	1.01	1.45	1.96	fitted
yellow	0.52	1.01	1.46	2.00	variations
cyan	0.51	1.00	1.45	1.90	partially
magenta	0.51	1.00	1.47	1.95	fitted
yellow	0.51	1.00	1.53	2.06	variations

B. Original extended CY model. Prediction accuracy for prints C2M2Y2, C4M4Y4, C6M6Y6 and C8M8Y8, when not considering volume variations.

dot-size	2	4	6	8	
mean ΔE_{94}	0.44	0.61	2.03	3.14	reference
std ΔE_{94}	0.29	0.38	1.69	2.55	
mean ΔE_{94}	23.55	1.01	8.41	15.04	no volume
std ΔE_{94}	4.46	0.79	4.39	7.44	variations

C. Thickness extended CY model. Prediction accuracy for prints C2M2Y2, C4M4Y4, C6M6Y6 and C8M8Y8, using nominal, fully fitted and partially fitted volume variations.

dot-size	2	4	6	8	
mean ΔE_{94}	0.72	1.01	2.68	3.76	reference
std ΔE_{94}	0.39	0.79	2.14	2.70	
mean ΔE_{94}	1.26	1.01	3.18	6.39	nominal
std ΔE_{94}	0.62	0.79	3.18	5.88	variations
mean ΔE_{94}	1.23	1.00	3.17	6.42	fully fitted
std ΔE_{94}	0.62	0.82	3.26	5.94	variations
mean ΔE_{94}	1.42	1.01	3.27	6.51	partially fitted
std ΔE_{94}	0.74	0.79	3.34	6.12	variations

References

[1] R. Balasubramanian. Optimization of the spectral neugebauer model for printer characterization. *Journal of Electronic Imaging*, 8(2):156–166, 1999.

[2] FR Clapper and JAC Yule. The effect of multiple internal reflections on the densities of halftone prints on paper. *Journal of the Optical Society of America*, 43(7):600–603, 1953.

[3] R.D. Hersch, M. Brichon, T. Bugnon, F. Amrhyn, F. Crété, S. Mourad, H. Janser, Y. Jiang, and M. Riepenhoff. Deducing ink thickness variations by a spectral prediction model. *Color Research and Applications*, in press.

[4] R.D. Hersch, P. Emmel, F. Collaud, and F. Crété. Spectral reflection and dot surface prediction models for color halftone prints. *Journal of Electronic Imaging*, 14:33001–12, 2005.

[5] H.E.J. Neugebauer. Die theoretischen Grundlagen des Mehrfarben-drucks. *Zeitschrift fuer wissenschaftliche Photographie*, 36:36–73, 1937.

[6] JL Saunderson. Calculation of the Color of Pigmented Plastics. *J. Opt. Soc. Amer*, 32(4):727–736, 1942.

[7] L. Yang. Characterization of inks and ink application for ink-jet printing: model and simulation. *Journal of the Optical Society of America A*, 20(7):1149–1154, 2003.

[8] L. Yang and B. Kruse. Ink penetration and its effects on printing. *IS&T/SPIE Conf. on Color Imaging: Device-Independent Color, Color Hardcopy and Graphic Arts V*, SPIE-Vol. 3963:365–375, 2000.

Author Biography

Fabrice Rousselle received his engineering degree from the Ecole Polytechnique de Montréal, Canada in 2000 and his MS degree from Université de Montréal, Canada in 2007. He is now a PhD student at the Peripheral Systems Laboratory of the Ecole Polytechnique Fédérale de Lausanne (EPFL), Switzerland. He is interested in computer graphics and in modeling the interaction of light, inks and paper.